INSTITUTE OF PHYSICS PUBLISHING WAVES IN RANDOM MEDIA

Waves Random Media **13** (2003) 137–149 PII: S0959-7174(03)58562-7

A study of the higher-order small-slope approximation for scattering from a Gaussian rough surface

M S Gilbert and J T Johnson

Department of Electrical Engineering and ElectroScience Laboratory, The Ohio State University, 205 Dreese Labs, 2015 Neil Ave, Columbus, OH 43210, USA

E-mail: gilbert.137@osu.edu and johnson@ee.eng.ohio-state.edu

Received 20 January 2003
Published 28 March 2003
Online at stacks.iop.org/WRM/13/137

Abstract

Results from the first three terms of the small-slope approximation (SSA) for incoherent electromagnetic scattering from a penetrable randomly rough interface are discussed. Surface roughness is characterized as a Gaussian random process with an isotropic Gaussian correlation function. Sample results illustrate parameter spaces for which each correction term is appreciable. Reduction of the SSA to the physical optics theory is also discussed for both perfectly conducting and dielectric surfaces.

1. Introduction

Predicting scattering cross sections of randomly rough surfaces is critical for designing terrain and sea surface remote sensing systems and interpreting the resulting data. The standard physical optics (PO) and small-perturbation methods (SPM) [1] have been applied extensively, but are limited in their applicability. Recent decades have seen continued development of improved theories, including the small-slope approximation (SSA) [2]. The first SSA incoherent scattering cross section term can be regarded as second order in surface 'quasi-slope' [3], and has a form similar to the PO approximation but multiplied by an alternative function of the surface permittivity and of the incident and scattering angles. This 'quasi-slope' designation highlights the fact that the SSA is considered a slope expansion for large-scale surface roughness, yet concurrently it reduces to a small height expansion for small-scale surface roughness. A recent paper [4] investigated the accuracy of the first SSA term through comparison with numerical simulations and found inaccuracies in the PO limit. However, [2] demonstrates that the SSA reproduces the PO theory when higher-order SSA corrections (at third and partial fourth order) are included in the scalar, hard-boundary scattering problem. The first two terms of the SSA series have also been shown to reduce to the 'two-scale' limit for multi-scale surfaces [5].

The second SSA term (third order) has a more complicated form involving a quadruple integral for computation of average incoherent cross sections, while the third SSA term (partial

fourth order) computation involves a sixfold integral. Expressions for the averages of all three SSA terms in the scalar, hard-boundary problem have been provided in [6] for 2D scattering problems and in [7] for 3D scattering problems. Averages of all three SSA terms can also be computed through a Monte Carlo simulation with a deterministic surface algorithm [8, 9]. The complexity of both the analytically averaged and Monte Carlo approaches, however, has limited the number of studies reported including the second and third SSA terms in the electromagnetic, penetrable surface problem. Recently, some results from the second and third SSA terms have been illustrated in [10] and [11], but simplified forms for Gaussian correlation function surfaces were not described.

In this paper, simplified forms for the first three SSA terms are presented for penetrable surfaces under the assumption of a Gaussian random process surface with an isotropic Gaussian correlation function. While these surfaces are admittedly simple compared to many natural surface structures, the isotropic Gaussian correlation function surface remains a widely used model in many applications. Surfaces in this case are described simply by the rms height h and correlation length l parameters, and the surface rms slope is related to the ratio h/l. Results for each SSA term are presented as the surface statistics and scattering geometry are varied to provide some information on the rate of convergence of the SSA series. Reduction of the three-term SSA series to the PO limit is also considered.

2. General formulation

Consider an incident time-harmonic plane wave with propagation vector $\boldsymbol{k}_\mathrm{i} = \hat{x}k_\mathrm{xi} + \hat{y}k_\mathrm{yi} - \hat{z}k_\mathrm{zi}$ impinging upon a rough interface between free space (permittivity ϵ_0 and permeability μ_0) and a dielectric medium (permittivity $\epsilon_1 = \epsilon_r\epsilon_0$ and permeability μ_0). The rough interface is defined as $z = f(x, y)$, with the z direction pointing upward into the free space region. Electromagnetic interactions with the rough surface create scattered fields on both sides of the interface. Observations made for scattered waves in the free space region with propagation vectors $\boldsymbol{k}_\mathrm{s} = \hat{x}k_\mathrm{xs} + \hat{y}k_\mathrm{ys} + \hat{z}k_\mathrm{zs}$ are described here. The incident and scattered propagation vector directional components can be defined in terms of the incident and scattered polar ($\theta_{\mathrm{i,s}}$) and azimuthal ($\phi_{\mathrm{i,s}}$) angles as

$$k_\mathrm{xi} = k\sin(\theta_\mathrm{i})\cos(\phi_\mathrm{i}) \qquad k_\mathrm{xs} = k\sin(\theta_\mathrm{s})\cos(\phi_\mathrm{s}) \tag{1}$$

$$k_\mathrm{yi} = k\sin(\theta_\mathrm{i})\sin(\phi_\mathrm{i}) \qquad k_\mathrm{ys} = k\sin(\theta_\mathrm{s})\sin(\phi_\mathrm{s}) \tag{2}$$

$$k_\mathrm{zi} = k\cos(\theta_\mathrm{i}) \qquad k_\mathrm{zs} = k\cos(\theta_\mathrm{s}) \tag{3}$$

where $k = 2\pi/\lambda$ is the wavenumber of an incident time-harmonic field at wavelength λ.

Following the notation of [7], the incoherent averaged normalized radar cross section for the dielectric Gaussian random process surface 3D scattering problem is written as a series of the first three SSA terms $\sigma_{\alpha\beta} \approx \sigma^{00}_{\alpha\beta} + \sigma^{01}_{\alpha\beta} + \sigma^{11}_{\alpha\beta}$. These three terms result from the first two terms in the SSA field solution, and are second-, third- and partial fourth-order results in surface 'quasi-slope', as described in [3, 6]. The $(\alpha\beta)$ subscripts refer to the polarizations (H for horizontal or V for vertical) of the scattered and incident fields respectively.

Expressions for these quantities can be derived following [2] and [6, 7] as

$$\sigma^{00}_{\alpha\beta} = \frac{k^2_\mathrm{zs}}{\pi k^2_\mathrm{dz}} |g^{(1)}_{\alpha\beta}(k_\mathrm{xs}, k_\mathrm{ys})|^2 \mathcal{H}\{1\} \tag{4}$$

$$\sigma^{01}_{\alpha\beta} = -\frac{k^2_\mathrm{zs}}{\pi |k_\mathrm{dz}|} \mathrm{Re}\{\mathrm{i}g^{(1)}_{\alpha\beta}(k_\mathrm{xs}, k_\mathrm{ys})[\mathcal{H}\{Q_{\alpha\beta}(x, y)\} + \mathrm{e}^{-k^2_\mathrm{dz}h^2}\mathcal{F}\{Q_{\alpha\beta}(x, y)\} - Q_{\alpha\beta}(0, 0)\mathcal{H}\{1\}]\} \tag{5}$$

$$\sigma_{\alpha\beta}^{11} = \frac{k_{\mathrm{zs}}^2}{4\pi k_{\mathrm{dz}}^2}\{[\mathcal{H}\{V_{\alpha\beta}(x,y)\} + \mathrm{e}^{-k_{\mathrm{dz}}^2 h^2}\mathcal{F}\{V_{\alpha\beta}(x,y)\} + k_{\mathrm{dz}}^2 |Q_{\alpha\beta}(0,0)|^2 \mathcal{H}\{1\}]\}. \tag{6}$$

The $g_{\alpha\beta}^{(1)}(k_{\mathrm{xs}}, k_{\mathrm{ys}})$ terms above are the first-order small-perturbation method (SPM) kernels, defined in [12] (equations (75), (76) for horizontal incident polarization and equations (79), (80) for vertical incident polarization). These kernels also depend on the incident wavevector and ϵ_r, although this dependence is not notated in the above equations for simplicity. The operators $\mathcal{F}$ and $\mathcal{H}$ above are defined as

$$\mathcal{F}\{f(x,y)\} = \int_{-\infty}^{\infty} \mathrm{d}x \int_{-\infty}^{\infty} \mathrm{d}y\, \mathrm{e}^{\mathrm{i}k_{\mathrm{dx}}x}\mathrm{e}^{\mathrm{i}k_{\mathrm{dy}}y} f(x,y) \tag{7}$$

$$\mathcal{H}\{f(x,y)\} = \int_{-\infty}^{\infty} \mathrm{d}x \int_{-\infty}^{\infty} \mathrm{d}y\, \mathrm{e}^{\mathrm{i}k_{\mathrm{dx}}x}\mathrm{e}^{\mathrm{i}k_{\mathrm{dy}}y} D(x,y) f(x,y) \tag{8}$$

where the k_{dx}, k_{dy} and k_{dz} parameters are defined as the difference between the incident and scattered wavevector components,

$$\boldsymbol{k}_{\mathrm{d}} = \hat{x}k_{\mathrm{dx}} + \hat{y}k_{\mathrm{dy}} + \hat{z}k_{\mathrm{dz}} = \hat{x}(k_{\mathrm{xi}} - k_{\mathrm{xs}}) + \hat{y}(k_{\mathrm{yi}} - k_{\mathrm{ys}}) - \hat{z}(k_{\mathrm{zi}} + k_{\mathrm{zs}}). \tag{9}$$

The term $D(x,y)$ is given by

$$D(x,y) = \mathrm{e}^{-k_{\mathrm{dz}}^2 h^2 (1 - C(x,y))} - \mathrm{e}^{-k_{\mathrm{dz}}^2 h^2} \tag{10}$$

with $C(x,y)$ representing the surface correlation function. The term $V_{\alpha\beta}(x,y)$ is given by

$$\begin{aligned} V_{\alpha\beta}(x,y) = {} & Q_{\alpha\beta}^{(1)}(x,y) + k_{\mathrm{dz}}^2 Q_{\alpha\beta}(x,y) Q_{\alpha\beta}^{*}(-x,-y) \\ & - k_{\mathrm{dz}}^2 (Q_{\alpha\beta}(0,0) Q_{\alpha\beta}^{*}(-x,-y) + Q_{\alpha\beta}^{*}(0,0) Q_{\alpha\beta}(x,y)). \end{aligned} \tag{11}$$

Finally, the $Q_{\alpha\beta}(x,y)$ and $Q_{\alpha\beta}^{(1)}(x,y)$ functions above are given by two-dimensional Fourier transforms of the surface power spectrum, $W(k_x, k_y)$, and the SSA kernel functions $G_{\alpha\beta}(k_x, k_y)$

$$Q_{\alpha\beta}(x,y) = \int_{-\infty}^{\infty} \mathrm{d}k_x \int_{-\infty}^{\infty} \mathrm{d}k_y\, \mathrm{e}^{\mathrm{i}k_x x}\mathrm{e}^{\mathrm{i}k_y y} G_{\alpha\beta}^{*}(k_x,k_y) W(k_x,k_y) \tag{12}$$

$$Q_{\alpha\beta}^{(1)}(x,y) = \int_{-\infty}^{\infty} \mathrm{d}k_x \int_{-\infty}^{\infty} \mathrm{d}k_y\, \mathrm{e}^{\mathrm{i}k_x x}\mathrm{e}^{\mathrm{i}k_y y} |G_{\alpha\beta}(k_x,k_y)|^2 W(k_x,k_y) \tag{13}$$

where * denotes complex conjugation. The SSA kernel is defined by a combination of first- and second-order SPM kernels [2]

$$\begin{aligned} G_{\alpha\beta}(k_x,k_y) = {} & g_{\alpha\beta}^{(2)}(k_{\mathrm{xs}}, k_{\mathrm{ys}}, k_{\mathrm{xi}} + k_x, k_{\mathrm{yi}} + k_y) + \mathrm{i}(k_{\mathrm{zs}} + k_{\mathrm{zi}}) g_{\alpha\beta}^{(1)}(k_{\mathrm{xs}}, k_{\mathrm{ys}}) \\ & + g_{\alpha\beta}^{(2)}(k_{\mathrm{xs}}, k_{\mathrm{ys}}, k_{\mathrm{xs}} - k_x, k_{\mathrm{ys}} - k_y) \end{aligned} \tag{14}$$

where the first-order SPM kernels are as explained above and the second-order SPM kernels, $g_{\alpha\beta}^{(2)}(k_{\mathrm{xs}}, k_{\mathrm{ys}}, k_{\mathrm{xn}}, k_{\mathrm{ym}})$, are defined in [12] (equations (88) and (89) for horizontal incident polarization and equations (95) and (96) for vertical incident polarization).

The preceding expressions apply for any Gaussian random process surface, regardless of its correlation function. The integration in equation (4) above is identical to that in PO theory, but the functions multiplying the integration are distinct in the SSA and PO cases. Note that equation (4) involves a double integration, while equations (5) and (6) involve quadruple and sixfold integrations, respectively, due to the Q functions involved. However, these computations can be made relatively efficient even for general surfaces if a fast-Fourier-transform (FFT) operation is used to tabulate the Q and $Q^{(1)}$ functions before proceeding to the spatial integrations. For specific correlation functions, further analytical forms for these equations can be derived.

3. Simplification for isotropic Gaussian correlation function

Consider a surface with an isotropic Gaussian correlation, defined as

$$C(x, y) = \exp\left[-\frac{x^2 + y^2}{l^2}\right] = C(\rho) \tag{15}$$

where the final equality assumes the use of standard cylindrical coordinates. The corresponding power spectrum in cylindrical coordinates is

$$W(k_\rho) = \frac{h^2 l^2}{4\pi} \exp\left[-\frac{l^2 k_\rho^2}{4}\right]. \tag{16}$$

Simplifications for equations (4)–(6) are based on the following steps: the spatial integration in each equation is first converted to cylindrical coordinates (ρ, ϕ), and the definition $k_{\mathrm{dx}} = k_{\mathrm{d}\rho} \cos(\phi')$, $k_{\mathrm{dy}} = k_{\mathrm{d}\rho} \sin(\phi')$ is made. The term

$$\mathrm{e}^{\mathrm{i}k_{\mathrm{d}\rho}\rho\cos(\phi-\phi')} = \sum_{u=-\infty}^{\infty} \mathrm{i}^u J_u(k_{\mathrm{d}\rho}\rho)\mathrm{e}^{\mathrm{i}u(\phi-\phi')} \tag{17}$$

then appears in all spatial integrations; the series expansion on the right-hand side above is from [13], where $J_u(k_{\mathrm{d}\rho}\rho)$ is the uth-order Bessel function of the first kind. Applying this expansion enables the integrations over ϕ to be expressed in terms of Fourier azimuthal harmonics. An additional power series expansion

$$\mathrm{e}^{-k_{\mathrm{dz}}^2 h^2 (1-C(\rho))} = \mathrm{e}^{-k_{\mathrm{dz}}^2 h^2} \sum_{n=0}^{\infty} \frac{(k_{\mathrm{dz}} h)^{2n}}{n!} \exp\left[\frac{-n\rho^2}{l^2}\right] \tag{18}$$

is also frequently used. Note that the above power series expansion will converge most rapidly for surfaces with moderate rms heights in terms of the electromagnetic wavelength. For small slope surfaces with larger heights, the large-scale expansion discussed in section 5 is more appropriate.

3.1. First SSA term

The above steps combined with the integral identity [13]

$$\int_0^\infty \mathrm{d}\rho\, \rho J_0(k_{\mathrm{d}\rho}\rho) \exp\left[\frac{-n\rho^2}{l^2}\right] = \frac{l^2}{2n} \exp\left[-\frac{k_{\mathrm{d}\rho}^2 l^2}{4n}\right] \tag{19}$$

are sufficient to reduce equation (4) to

$$\begin{aligned}\sigma_{\alpha\beta}^{00} &= \frac{k_{\mathrm{zs}}^2}{\pi k_{\mathrm{dz}}^2} |g_{\alpha\beta}^{(1)}(k_{\mathrm{xs}}, k_{\mathrm{ys}})|^2 \left(\pi l^2 \mathrm{e}^{-k_{\mathrm{dz}}^2 h^2} \sum_{n=1}^{\infty} \frac{(k_{\mathrm{dz}}^2 h^2)^n}{n!n} \mathrm{e}^{-k_{\mathrm{d}\rho}^2 l^2/(4n)}\right) \\ &= \frac{k_{\mathrm{zs}}^2}{\pi k_{\mathrm{dz}}^2} |g_{\alpha\beta}^{(1)}(k_{\mathrm{xs}}, k_{\mathrm{ys}})|^2 D_{\mathrm{I}}.\end{aligned} \tag{20}$$

The D_{I} term defined above is identical to that from [1] obtained in simplifying PO theory results, except a term involving the surface area in [1] is not included. Convergence of this series requires $n \gg (k_{\mathrm{dz}} h)^2$. Note that numerical problems in computing D_{I} single terms for large n can be reduced by first adding and subtracting the logarithms of factors making up the term, followed by exponentiation of the result.

3.2. Second SSA term

Simplifying the second SSA term requires that the Q function first be written as

$$Q_{\alpha\beta}(\rho,\phi) = \sum_{m=-\infty}^{\infty} \mathrm{i}^m \mathrm{e}^{-\mathrm{i}m\phi} \int_0^{\infty} \mathrm{d}k_\rho\, k_\rho W(k_\rho) J_m(k_\rho\rho) \tilde{G}_{m,\alpha\beta}(k_\rho) \tag{21}$$

through the use of the steps described above, where

$$\tilde{G}_{m,\alpha\beta}(k_\rho) = \int_0^{2\pi} \mathrm{d}\tilde{\phi}\, \mathrm{e}^{\mathrm{i}m\tilde{\phi}} G^*_{\alpha\beta}(k_\rho\cos\tilde{\phi}, k_\rho\sin\tilde{\phi}) \tag{22}$$

are the azimuthal Fourier harmonics of the conjugated SSA kernel. Due to the limited harmonic structure of $\tilde{G}_{\alpha\beta}$, the above series truncated to $m = \pm 8$ was found to produce cross sections accurate to within 0.3 dB for all cases illustrated.

Note that equation (5) is composed of three additive terms that can be simplified separately:

$$\sigma^{01}_{\alpha\beta} = -\frac{k_{\mathrm{zs}}^2}{\pi|k_{\mathrm{dz}}|} \mathrm{Re}\{\mathrm{i} g^{(1)}_{\alpha\beta}(k_{\mathrm{xs}}, k_{\mathrm{ys}})[A^{01}_1 + A^{01}_2 + A^{01}_3]\}. \tag{23}$$

Results after simplification are

$$A^{01}_1 = \pi l^2 \mathrm{e}^{-k_{\mathrm{dz}}^2 h^2} \sum_{n=1}^{\infty} \frac{(k_{\mathrm{dz}}h)^{2n}}{n!n} \sum_{m=-\infty}^{\infty} (-1)^m \mathrm{e}^{-\mathrm{i}m\phi'} B^{01}_{n,m} \tag{24}$$

$$A^{01}_2 = 4\pi^2 \mathrm{e}^{-k_{\mathrm{dz}}^2 h^2} G^*_{\alpha\beta}(-k_{\mathrm{dx}}, -k_{\mathrm{dy}}) W(k_{\mathrm{d}\rho}) \tag{25}$$

$$A^{01}_3 = -Q_{\alpha\beta}(0,0) D_{\mathrm{I}}. \tag{26}$$

Here $B^{01}_{n,m}$ is defined as

$$B^{01}_{n,m} = \int_0^{\infty} \mathrm{d}k_\rho k_\rho W(k_\rho) \tilde{G}_{m,\alpha\beta}(k_\rho) I_m\left[\frac{l^2 k_{\mathrm{d}\rho} k_\rho}{2n}\right] \exp\left[-\frac{l^2(k_{\mathrm{d}\rho}^2 + k_\rho^2)}{4n}\right] \tag{27}$$

where I_m is the mth-order modified Bessel function of the first kind. The integral identity [13]

$$\int_0^{\infty} \mathrm{d}\rho\, \rho J_m(k_{\mathrm{d}\rho}\rho) J_m(k_\rho\rho) \exp\left[\frac{-n\rho^2}{l^2}\right] = \frac{l^2}{2n} I_m\left[\frac{l^2 k_{\mathrm{d}\rho} k_\rho}{2n}\right] \exp\left[-\frac{l^2(k_{\mathrm{d}\rho}^2 + k_\rho^2)}{4n}\right] \tag{28}$$

is used in obtaining the final form of A^{01}_1, while the form for A^{01}_2 results from the fact that $\mathcal{F}$ is a Fourier transform operator. The form for A^{01}_1 has replaced a fourfold integral with a double sum of a single integral over the SSA kernel azimuthal harmonics. The single integral involved, however, is relatively well behaved given the net exponentially decaying behaviour exhibited by the integrand.

3.3. Third SSA term

Similar methods are used to simplify the third SSA term. The result is

$$\sigma^{11}_{\alpha\beta} = \frac{k_{\mathrm{zs}}^2}{4\pi k_{\mathrm{dz}}^2}[A^{11}_1 + A^{11}_2 + A^{11}_3] \tag{29}$$

where

$$A^{11}_1 = \left(\pi l^2 \mathrm{e}^{-k_{\mathrm{dz}}^2 h^2} \sum_{n=1}^{\infty} \frac{(k_{\mathrm{dz}}h)^{2n}}{n!n} \mathrm{Re}\left\{\sum_{m=-\infty}^{\infty} (-1)^m \mathrm{e}^{-\mathrm{i}m\phi'} B^{11}_{n,m}\right\}\right)$$
$$+ 2\pi k_{\mathrm{dz}}^2 \mathrm{e}^{-k_{\mathrm{dz}}^2 h^2} \sum_{n=0}^{\infty} \sum_{k=0}^{\infty} \sum_{m=-\infty}^{\infty} \sum_{v=-\infty}^{\infty} E_{k,v} E^*_{n,-m} D_{k+n,m,v} \tag{30}$$

$$A_2^{11} = 4\pi^2 \mathrm{e}^{-k_{\mathrm{dz}}^2 h^2} W(k_{\mathrm{d}\rho}) \left\{ |G_{\alpha\beta}(-k_{\mathrm{dx}}, -k_{\mathrm{dy}})|^2 - 2k_{\mathrm{dz}}^2 \mathrm{Re}\{Q_{\alpha\beta}(0,0) G_{\alpha\beta}(-k_{\mathrm{dx}}, -k_{\mathrm{dy}})\} \right\}$$
$$+ 8\pi^2 k_{\mathrm{dz}}^2 \mathrm{e}^{-k_{\mathrm{dz}}^2 h^2} \mathrm{e}^{-k_{\mathrm{d}\rho}^2 l^2/8} \int_0^\infty \mathrm{d}k_\rho \, k_\rho W^2(k_\rho)$$
$$\times \ \mathrm{Re}\left\{ \int_0^\pi \mathrm{d}\phi \, G_{\alpha\beta}^*\left(-\frac{k_{\mathrm{dx}}}{2} + k_\rho \cos(\phi), -\frac{k_{\mathrm{dy}}}{2} + k_\rho \sin(\phi) \right) \right.$$
$$\left. \times \ G_{\alpha\beta}\left(-\frac{k_{\mathrm{dx}}}{2} - k_\rho \cos(\phi), -\frac{k_{\mathrm{dy}}}{2} - k_\rho \sin(\phi) \right) \right\} \tag{31}$$

$$A_3^{11} = k_{\mathrm{dz}}^2 |Q_{\alpha\beta}(0,0)|^2 D_I. \tag{32}$$

In A_1^{11}, the $B_{n,m}^{11}$ function is identical to $B_{n,m}^{01}$ except that

$$|G_{\alpha\beta}(k_x, k_y)|^2 - 2k_{\mathrm{dz}}^2 Q_{\alpha\beta}^*(0,0) G_{\alpha\beta}^*(k_x, k_y) \tag{33}$$

is used instead of $G_{\alpha\beta}^*(k_x, k_y)$ to determine the Fourier series terms $\tilde{G}_{m,\alpha\beta}(k_\rho)$. Also, $D_{a,b,c}$ from the A_1^{11} component is given as follows:

$$D_{a,b,c} = \frac{(-1)^a (\mathrm{sgn}(b+c))^{|b+c|}}{2^{2a+|b|+|c|}} \int_0^\infty \mathrm{d}\rho \, \rho^{2a+|b|+|c|+1} J_{|b+c|}(k_{\mathrm{d}\rho}\rho) [\mathrm{e}^{k_{\mathrm{dz}}^2 h^2 C(\rho)} - 1] \tag{34}$$

while $E_{a,b}$ is given by

$$E_{a,b} = (-\mathrm{sgn}(b))^{|b|} \frac{\mathrm{e}^{-\mathrm{i}b\phi'}}{a!(a+|b|)!} \int_0^\infty \mathrm{d}k_\rho \, k_\rho^{2a+|b|+1} W(k_\rho) \tilde{G}_{b,\alpha\beta}(k_\rho). \tag{35}$$

Here the sgn operator produces the sign (i.e. ± 1) of its argument, with argument zero producing a result of +1. Note that A_1^{11} above contains terms similar to those in A_1^{01}, but the additional fourfold sums result from the $Q(x, y)Q^*(-x, -y)$ contribution in $V(x, y)$. The final form obtained for this contribution is based on an additional power series expansion of the Bessel functions in the Q function azimuthal series (equation (21)). The result for A_2^{11} again follows from the Fourier transform properties of $\mathcal{F}$: the integral term is the convolution theorem for the $Q(x, y)Q^*(-x, -y)$ contribution.

In the above equations, the most expensive computation involves the fourfold sum of the E and D function integrals. However, again the simplification has produced relatively well behaved E integrals because of the power spectrum exponential dependence. The E functions can also be tabulated before proceeding to the fourfold sum to improve efficiency; limiting the m and v sums to ± 8 again was found to produce cross sections accurate to within 0.3 dB for all cases illustrated. For the n and k summations (from the series representation of the Bessel functions), the number of terms included is increased until convergence to within 0.1% is observed. Typically these series converge in fewer than 40 terms for the cases illustrated. Note that the m summation for $B_{n,m}^{11}$ requires twice as many terms as the m and v summations in the fourfold sum due to the squared SSA kernel involved. The above equations were implemented, and results were tested for consistency through comparison with results from a Monte Carlo simulation of the SSA as described in [9]. Calculation of equations (23)–(35) at each angle executed in approximately 4 min on an 800 MHz Pentium processor (of which 99.9% was spent on the third SSA term).

4. Results

Figures 1 and 2 illustrate backscattered σ^{00}, σ^{01} and σ^{11} from equations (20)–(35) in the $kh = 0.5, kl = 3$ and $kh = 1, kl = 6$ cases, respectively. These surfaces have identical slopes, and rms heights that exceed the limitations of standard perturbation theory; the former case

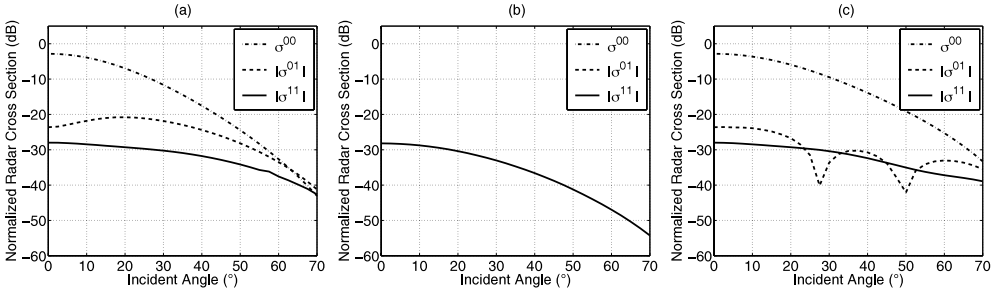

Figure 1. Backscattering: σ^{00}, σ^{01} and σ^{11}; $kh = 0.5$, $kl = 3$, $\epsilon_r = 4 + i$; (a) HH; (b) HV/VH; (c) VV.

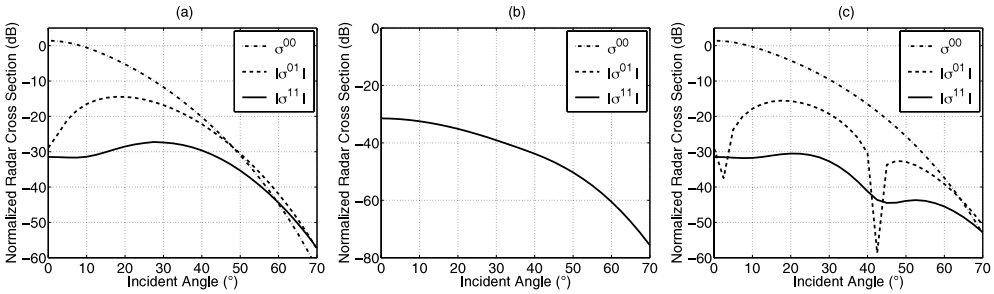

Figure 2. Backscattering: σ^{00}, σ^{01} and σ^{11}; $kh = 1$, $kl = 6$, $\epsilon_r = 4 + i$; (a) HH; (b) HV/VH; (c) VV.

is a smaller-height example, while the latter case has a height standard deviation approaching one wavelength. The three plots (a)–(c) in each figure are for HH, HV/VH and VV returns, respectively, for surfaces with relative permittivity $4 + i$. The second and third SSA terms are observed to be more important in HH returns, becoming significant for incidence angles larger than approximately 30°. A sign-change in the second VV SSA term produces the oscillatory behaviours observed, and an increased importance of the third SSA term is also present in the smaller-height case. Cross polarized predictions are obtained only from the third SSA term, because the first-order SPM kernel vanishes for backscattered cross-pol SSA fields at first-order. The computation of the third SSA term for backscattered cross-pol results is somewhat simplified because both $G_{\alpha\beta}(-k_{\mathrm{dx}}, -k_{\mathrm{dy}})$ and $Q_{\alpha\beta}(0, 0)$ vanish in this case. Also, for backscattered cross-pol results it can be shown that $\tilde{G}_{m,\alpha\beta} = -\tilde{G}_{-m,\alpha\beta}$ in the E integrations, and that $B^{11}_{n,m} = B^{11*}_{n,-m}$. Comparisons of all these results with first-order SPM predictions show poor agreement in general; the PO theory provides reasonable accuracy in the $kh = 1$, $kl = 6$ co-pol case but poor agreement (particularly for HH polarization) in the smaller scale roughness case.

To study convergence of the SSA series, the following quantities are defined:

$$\sigma^{(2)}_{\alpha\beta} = \sigma^{00}_{\alpha\beta} \tag{36}$$

$$\sigma^{(3)}_{\alpha\beta} = \sigma^{00}_{\alpha\beta} + \sigma^{01}_{\alpha\beta} \tag{37}$$

$$\sigma^{(4)}_{\alpha\beta} = \sigma^{00}_{\alpha\beta} + \sigma^{01}_{\alpha\beta} + \sigma^{11}_{\alpha\beta}. \tag{38}$$

Note that $\sigma^{01}_{\alpha\beta}$ can be either positive or negative, so that cross sections can decrease in some cases as this term is added.

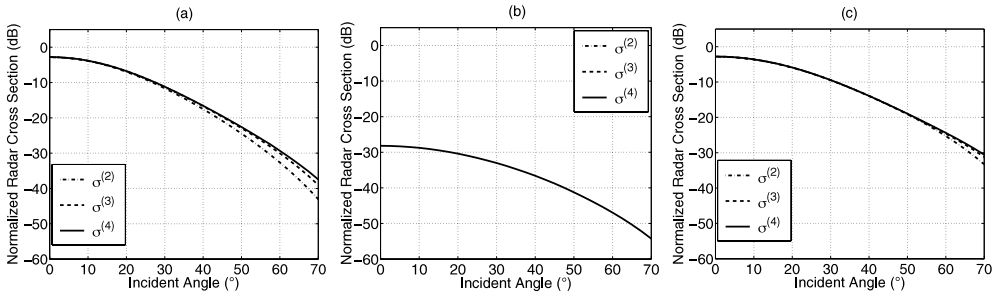

Figure 3. Backscattering: $\sigma^{(2)}$, $\sigma^{(3)}$ and $\sigma^{(4)}$; $kh = 0.5$, $kl = 3$, $\epsilon_r = 4+i$; (a) HH; (b) HV/VH; (c) VV.

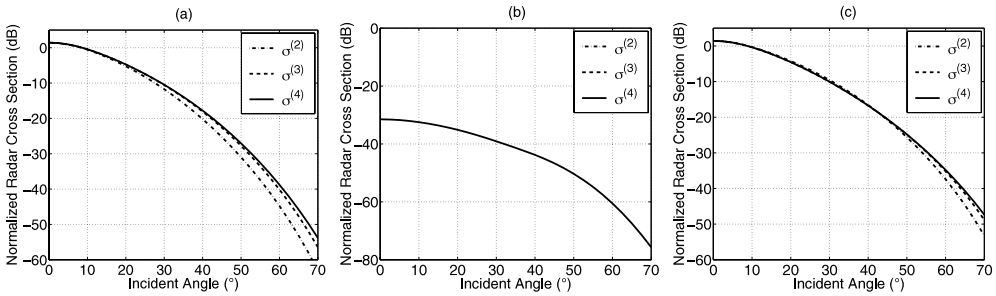

Figure 4. Backscattering: $\sigma^{(2)}$, $\sigma^{(3)}$ and $\sigma^{(4)}$; $kh = 1$, $kl = 6$, $\epsilon_r = 4 + i$; (a) HH; (b) HV/VH; (c) VV.

Figures 3 and 4 plot backscattered HH, HV/VH and VV polarized $\sigma^{(2)}_{\alpha\beta}$, $\sigma^{(3)}_{\alpha\beta}$ and $\sigma^{(4)}_{\alpha\beta}$ results for the $kh = 0.5$, $kl = 3$ and $kh = 1$, $kl = 6$ cases, respectively, at multiple incidence angles. Again the second and third SSA terms are seen to be more important at larger incidence angles, where an appreciable change in total cross sections is produced. The effect is largest in HH polarization in the larger-surface-height case. Figure 5 illustrates in-plane bistatic HH, HV, VH and VV polarized results for the $kh = 1$, $kl = 6$ case at 30° incidence angle. As can be seen, at angles farther from specular (scattering angle equal to 30° is the specular direction), the higher-order terms become more appreciable.

To study further the importance of the second and third SSA series terms, calculations using equations (20)–(35) were performed for kh values of $0.1, 0.2, \ldots, 1.5$ and kl values of $1, 2, \ldots, 10$. Computations were performed for this grid so long as the h/l values were strictly less than 0.3. In this study, the surface dielectric constant was fixed at $\epsilon_r = 4 + i$ and backscattering at incidence angles of 30° and 70° was considered. The results of figures 3 and 4 suggest defining third- and fourth-order 'improvements' as $|\sigma^{(3)}_{\alpha\beta,\mathrm{d}B} - \sigma^{(2)}_{\alpha\beta,\mathrm{d}B}|$ and $|\sigma^{(4)}_{\alpha\beta,\mathrm{d}B} - \sigma^{(3)}_{\alpha\beta,\mathrm{d}B}|$, respectively, where the dB subscript indicates quantities in decibels. Figures 6–9 illustrate third- (plot(a)) and fourth-order (plot (b)) improvements for HH and VV polarizations at incidence angles of 30° and 70°. Results for 30° incidence (figures 6 and 7) show relatively minor contributions (less than 2 dB everywhere) for the second and third SSA terms, although the corrections are more important in HH polarization than VV. Corrections are much more important in the 70° incidence case (figures 8 and 9), with values up to 20 dB observed. Note in all these figures that the corrections show a complex dependence in kh, kl space that is not a function only of h/l. This is due to the 'quasi-slope' nature of the SSA series [3], primarily due to the fact that the single-term SSA solution for dielectric surfaces

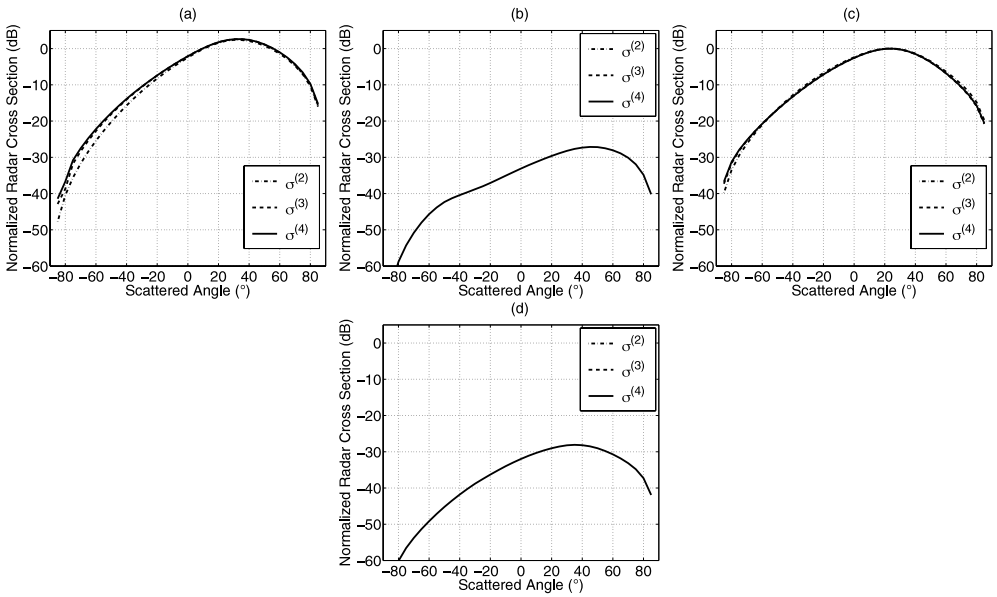

Figure 5. Bistatic scattering: 30° incidence, $\sigma^{(2)}$, $\sigma^{(3)}$ and $\sigma^{(4)}$; $kh = 1$, $kl = 6$, $\epsilon_r = 4 + i$; (a) HH, (b) HV, (c) VV and (d) VH.

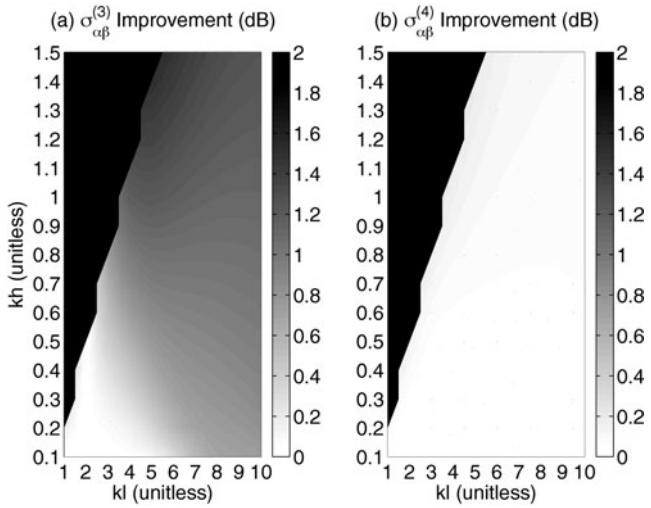

Figure 6. Backscattering improvements, HH polarization, $\epsilon_r = 4 + i$, $\theta_i = 30°$, (a) third order and (b) fourth order.

reduces exactly to the first-order SPM solution in the small-height limit, but only approaches PO in the large-height limit as more terms are included. The next section discusses this point further.

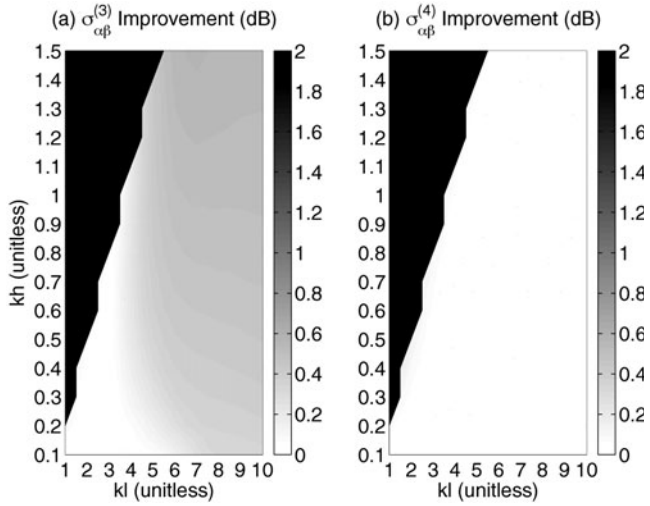

Figure 7. Backscattering improvements, VV polarization, $\epsilon_r = 4 + i$, $\theta_i = 30°$, (a) third order, (b) fourth order.

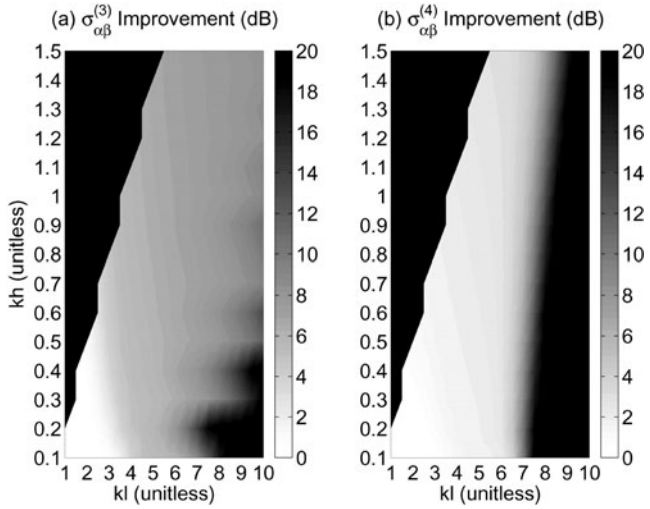

Figure 8. Backscattering improvements, HH polarization, $\epsilon_r = 4 + i$, $\theta_i = 70°$, (a) third order, (b) fourth order.

5. Large-scale roughness

A 'large-scale' surface approximation for the second and third SSA terms can be derived by expanding the SSA kernel in a Taylor series about the origin

$$G_{\alpha\beta}(k_x, k_y) \approx k_x G_{k_x} + k_y G_{k_y} \tag{39}$$

where $G_{k_x} = \frac{\partial G_{\alpha\beta}(k_x,k_y)}{\partial k_x}$ is the partial of the general SSA kernel (14) with respect to k_x, and $G_{k_y} = \frac{\partial G_{\alpha\beta}(k_x,k_y)}{\partial k_y}$ is the partial with respect to k_y, both evaluated at the origin. Utilizing this reduction and steps similar to those described previously, equations (23) and (29) can be

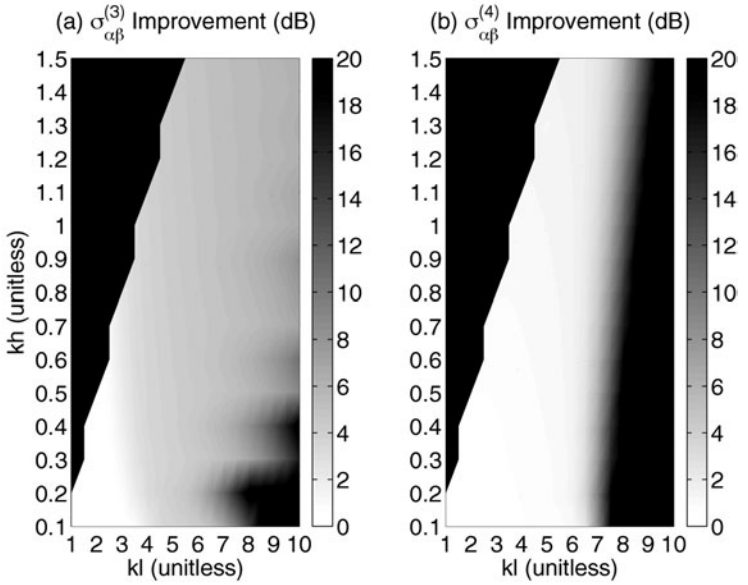

Figure 9. Backscattering improvements, VV polarization, $\epsilon_r = 4 + i$, $\theta_i = 70°$, (a) third order, (b) fourth order.

simplified to

$$\sigma_{\alpha\beta}^{01} \approx -\frac{k_{\mathrm{zs}}^2 D_{\mathrm{I}}}{\pi |k_{\mathrm{dz}}|} \operatorname{Re}\left\{ \mathrm{i} g_{\alpha\beta}^{(1)}(k_{\mathrm{xs}}, k_{\mathrm{ys}}) \frac{k_{\mathrm{d}\rho}}{|k_{\mathrm{dz}}|^2} [G_{k_x}^* \cos(\phi') + G_{k_y}^* \sin(\phi')] \right\} \tag{40}$$

$$\sigma_{\alpha\beta}^{11} \approx \frac{k_{\mathrm{zs}}^2 D_{\mathrm{I}}}{4\pi k_{\mathrm{dz}}^2} \left\{ \frac{k_{\mathrm{d}\rho}^2}{2k_{\mathrm{dz}}^2} [|G_{k_x}|^2 (1 + \cos(2\phi')) + |G_{k_y}|^2 (1 - \cos(2\phi')) + 2 \operatorname{Re}\{G_{k_x} G_{k_y}^*\} \sin(2\phi')] \right\} \tag{41}$$

where the D_I term is as defined previously. Note that in this limit, all three SSA series terms are expressed as D_{I} times a function of angle; all surface parameter dependences are inside the D_{I} sum. Because PO theory results have a similar form [1], the sum of the three SSA terms can be compared to PO predictions for all surface statistics simply by comparing the angular functions multiplying D_{I}. Writing

$$\sigma_{\alpha\beta}^{(2)} = F^{(2)}(k_{\mathrm{xi}}, k_{\mathrm{yi}}, k_{\mathrm{xs}}, k_{\mathrm{ys}}) k^2 D_{\mathrm{I}} \tag{42}$$

$$\sigma_{\alpha\beta}^{(3)} = F^{(3)}(k_{\mathrm{xi}}, k_{\mathrm{yi}}, k_{\mathrm{xs}}, k_{\mathrm{ys}}) k^2 D_{\mathrm{I}} \tag{43}$$

$$\sigma_{\alpha\beta}^{(4)} = F^{(4)}(k_{\mathrm{xi}}, k_{\mathrm{yi}}, k_{\mathrm{xs}}, k_{\mathrm{ys}}) k^2 D_{\mathrm{I}} \tag{44}$$

$$\sigma_{\alpha\beta}^{PO} = F^{PO}(k_{\mathrm{xi}}, k_{\mathrm{yi}}, k_{\mathrm{xs}}, k_{\mathrm{ys}}) k^2 D_{\mathrm{I}} \tag{45}$$

defines the angular F functions to be compared; the k^2 term extracted removes any explicit frequency dependence as well.

Figure 10 illustrates a comparison of these angular functions for backscattering from perfectly conducting surfaces, and demonstrates that $F^{(4)}$ becomes identical to F^{PO} to within the accuracy of the numerics. This reduction to PO results for the scalar, hard-boundary problem has previously been described in [2, 3]. $F^{(2)}$ and $F^{(3)}$ also match F^{PO} for small incidence angles, but can show large differences at larger observation angles. These results again show that matching the PO theory in the large-scale, perfectly-conducting-surface limit

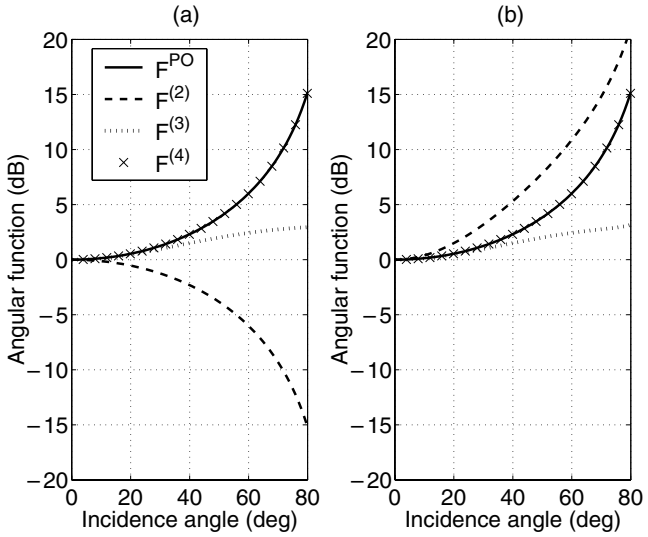

Figure 10. Comparison of SSA and PO angular functions: perfectly conducting surface, (a) HH, (b) VV.

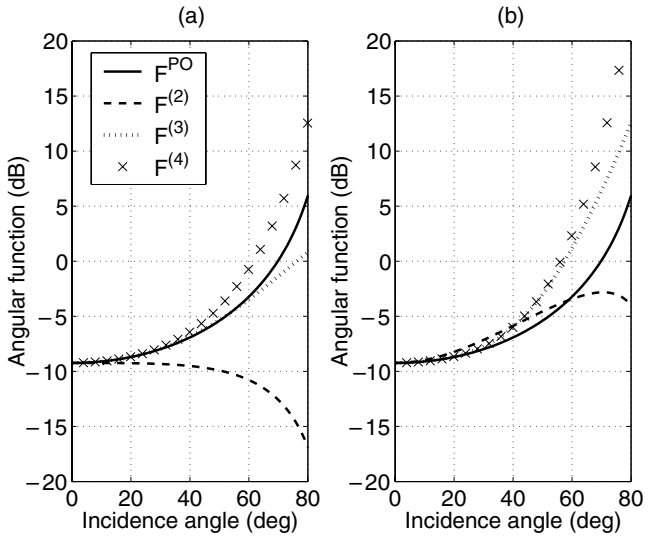

Figure 11. Comparison of SSA and PO angular functions: $\epsilon_r = 4 + i$, (a) HH, (b) VV.

requires inclusion of both the second and third SSA terms. The large 'improvement' factors found for larger surface heights in the previous section are produced by the large differences between the $F^{(2)}$–$F^{(4)}$ angular functions at larger observation angles.

Figure 11 illustrates the same comparison for surfaces with dielectric constant $\epsilon_r = 4 + i$. Again for small observation angles, all functions match, but large differences are observed at larger angles. In this case, $F^{(4)}$ and $F^{(PO)}$ remain distinct at larger angles, with $F^{(4)}$ typically exceeding $F^{(PO)}$. Note that evaluation of $F^{(PO)}$ for dielectric surfaces requires an approximation of the reflection coefficients involved: in the results presented, reflection coefficients were evaluated at the stationary phase point (i.e. zero degrees incidence for

backscattering). At present, it is unclear whether the large-scale approximated SSA or the stationary phase point PO theory is more appropriate for large-scale dielectric surfaces: further studies with more exact methods are required to address this issue.

6. Summary

In this paper, simplified forms for the first three terms in the SSA series for incoherent scattering from a Gaussian correlation function surface were presented. The resulting forms remained computationally complex, but simplified the forms of the integrations involved. Results showed the second and third terms to make important contributions, particularly at larger observation angles and for larger-height surfaces. An approximation to all three SSA terms in the 'large-scale' surface limit confirmed that the sum of the first three SSA terms becomes identical to the PO prediction for perfectly conducting surfaces. Results with dielectric surfaces however showed PO (using stationary phase point reflection coefficients) and the large-scale approximated SSA to produce significantly differing predictions at larger observation angles.

References

[1] Tsang L, Kong J A and Shin R T 1985 *Theory of Microwave Remote Sensing* (New York: Wiley)
[2] Voronovich A 1994 *Wave Scattering from Rough Surfaces* (Heidelberg: Springer)
[3] Broschat S L and Thorsos E I 1995 An investigation of the small slope approximation for scattering from rough surfaces: part I—theory *J. Acoust. Soc. Am.* **97** 2082–93
[4] Soriano G, Guerin C and Saillard M 2002 Scattering by two-dimensional rough surfaces: comparison between the method of moments, Kirchhoff, and small-slope approximations *Waves Random Media* **12** 63–83
[5] Voronovich A G 2002 The effect of the modulation of Bragg scattering in small-slope approximation *Waves Random Media* **12** 341–9
[6] Broschat S L and Thorsos E I 1997 An investigation of the small slope approximation for scattering from a rough surface: part II—numerical studies *J. Acoust. Soc. Am.* **101** 2615–25
[7] Yang T and Broschat S L 1992 A comparison of scattering model results for two-dimensional randomly rough surfaces *IEEE Trans. Antennas Propag.* **40** 1505–12
[8] Ewe H T, Johnson J T and Chen K S 2001 A comparison study of surface scattering models *IGARSS 2001 (Sydney) Conf. Proc.* vol 6 pp 2692–4
[9] McDaniel S 1999 Acoustic and radar scattering from directional seas *Waves Random Media* **9** 537–49
[10] Berginc G, Béniguel Y and Chevalier B 1999 Small slope approximation method: higher order contributions for scattering from conducting 3D surfaces *SPIE Conf. on Scattering and Surface Roughness (SPIE vol 3784)* (Bellingham, WA: SPIE) pp 207–17
[11] Voronovich A G and Zavorotny V U 2001 Theoretical model for scattering of radar signals in K-u- and C-bands from a rough sea surface with breaking waves *Waves Random Media* **11** 247–69
[12] Johnson J T 1999 Third order SPM for scattering from dielectric rough surfaces *J. Opt. Soc. Am.* **16** 2720–36
[13] Gradshteyn I S and Ryzhik I M 1994 *Table of Integrals, Series, and Products* 5th edn (London: Academic)